JOURNAL OF GEOPHYSICAL RESEARCH, VOL. 101, NO. B3, PAGES 5519–5530, MARCH 10, 1996

Marine controlled-source electromagnetic sounding 2. The PEGASUS experiment

S. Constable and C. S. Cox

Scripps Institution of Oceanography, University of California San Diego, La Jolla

Abstract. The marine controlled-source electromagnetic sounding method developed over the past 15 years at Scripps Institution of Oceanography employs a towed seafloor electric dipole transmitter of moment 4×10^4 Am and multiple free-vehicle seafloor electric field recorders. A survey of 40 Ma normal oceanic lithosphere in the northeast Pacific using frequencies of 0.25 to 24 Hz and synchronous stacking of 0.25- to 12-hour-duration detected signals at transmitter-receiver ranges between 5 and 95 km. One-dimensional electrical conductivity structure is recovered from the data using the Occam process of nonlinear regularized inversion. Repeated inversion of a model terminated with an essentially infinite conductor or resistor demonstrates that the maximum depth of inference for this experiment is about 30 km, well into the upper mantle, with bounds placed on conductivity to depths of 60 km. Structure shallower than about 1 km is comparable to that obtained by a similar experiment on the East Pacific Rise and by borehole logging, with a sharp increase in resistivity at depths of 600–800 m, although strictly our experiment is sensitive only to integrated square root of conductivity, or total attenuation, in the surface layers. The lower crust and upper mantle has a resistivity between 2 and 7×10^4 Ω m and a transverse resistance of at least 10^9 Ω m^2, suggesting at most 0.3% volume fraction of free water in the lower crust and some form of conductivity enhancement over mineral conductivity in the uppermost mantle. Although resolution is weak, below 30 km our data are compatible with a dry olvine model of mantle conductivity–temperature.

Introduction

In a companion paper, *Flosadottir and Constable* [this issue] describe the dipole-dipole seafloor controlled-source electromagnetic method, motivate its use in marine electrical studies, explain an efficient forward and inverse computation method for one-dimensional (1-D) models, and present a resolution analysis for normal oceanic lithosphere. The purpose of the present paper is to describe the experimental technique and present results from a survey carried out in the north east Pacific Ocean during November 1988. During this experiment, measurements were also made of seafloor pressure variations [*Webb et al.*, 1991] and seafloor gravity [*Zumberge et al.*, 1991], and so the acronym PEGASUS (Pressure, Electromagnetic, Gravity, Active Source Underwater Survey) was coined by one of our esteemed colleagues.

The experimental area, on 40 Ma lithosphere in the north east Pacific at 35°N, 132°W, was chosen to be representative of normal oceanic crust and mantle and for its mild topography, proximity to San Diego, and thin sediment cover. This location in particular was used because swath bathymetry data had been previously collected in a 50×50 km region as part of an experiment to determine any scale length dependence of the gravitational constant [*Zumberge et al.*, 1991], and we needed such a map for our transmitter tow. Depths varied between 4900 m and 5300 m over the survey region, with the dominant topography a 150-m-high ridge running north-south down the center of our array. As part of the gravity study, sediment thicknesses were obtained within the area using 4.5 kHz acoustic profiling along an approximately 150-km track (J. Hildebrand, personal communication, 1992). Sediment thickness varied between 11 and 87 m, with a modal value of about 35 m. There is no apparent correlation of sediment thickness with topography.

Paper number 95JB03738.
0148-0227/96/95JB-03738$05.00.

Experimental Method

The system described here uses a seafloor horizontal electric dipole source and a series of horizontal electric field receivers. This system is in use by both Scripps Institution of Oceanography and Cambridge University and has been described in part by *Webb et al.* [1985], *Constable* [1990], *Chave et al.* [1991], *Sinha et al.* [1990], and *Flosadottir and Constable* [this issue].

The objective of the transmitter design is to get as large a current as possible in the water at the seafloor through a 17-mm-diameter, armored RG8/U towing cable. To avoid ohmic losses in the cable, shipboard 60 Hz power is transformed up to the highest voltage the cable will endure (about 2000 V) and mixed with a 20 kHz control signal before being sent down the cable through a set of slip rings on the winch (Figure 1). At the seafloor the power is transformed back down to about 100 V, and a combination of full-wave rectification and polarity switching is accomplished by means of a bridge of silicon controlled rectifiers (SCRs), which are activated according to the control signal. In this way the final frequency of transmission is under continuous and complete control from the surface unit.

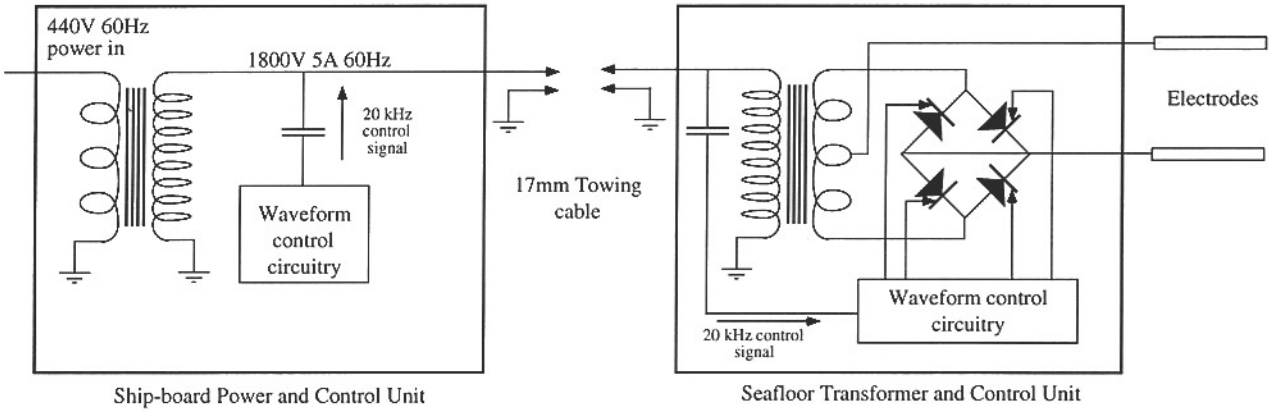

Figure 1. Block diagram of the controlled-source transmitter used in the experiments. High voltage, low current 60 Hz power is generated on board ship and passed via the towing cable to the seafloor transformer unit. There it is transformed to low voltage, high current and switched using a set of rectifiers to form a waveform with a lower frequency envelope.

During PEGASUS the control signals were designed to produce the waveform envelope shown in Figure 2a. Switching at time ϕ_1, ϕ_2, etc. modulated the quasi-dc current produced by the full-wave rectification of the nominally 60 Hz power. The high frequencies associated with the 120-Hz fundamental and overtones of the rectified current (Figure 2b) are undetectable by the seafloor receivers, and it is only the zero-frequency term that is important, or $2/\pi$ times the peak amplitude of the arches. Since the peak amplitude is $1/\sqrt{2}$ times the unrectified RMS current, the final DC signal is $2\sqrt{2}/\pi$ or 0.900 times the RMS supply.

Because the envelope shown in Figure 2a is symmetric about zero and antisymmetric about $\pi/2$, it can be expressed in the frequency domain as a cosine series of only odd terms. These harmonics have values

$$b_n = \frac{4}{\pi n}(\sin n\phi_1 - \sin n\phi_2), \quad n = 1, 3, 5, \cdots. \tag{1}$$

For PEGASUS, ϕ_1 was set to 22.0° and ϕ_2 was set to 83.5°, to give first and third harmonics of equal amplitude and little power in higher harmonics. The amplitudes,

$$\mathbf{b} = 0.788, -0.788, -0.024, -0.208, 0.119, 0.064 \cdots \tag{2}$$

are shown graphically in Figure 2c. Equal first and third harmonics are a convenient way to transmit two frequencies at the same time and provide improved ability to discriminate signal from spurious effects.

A total of 1450 V_{RMS} and 6.3 A_{RMS} were applied to the towing cable by the secondary of the shipboard transformer; ohmic and capacitive losses in the cable (51 Ω and 0.72 μF) reduced these values to 1150 V_{RMS} and 5.9 A_{RMS} at the seafloor. The underwater transformer has a turns ratio of 17:1, and so we infer 100 A_{RMS} and 67.5 V_{RMS} available to the SCR bridge. About 3.5 V was dropped across the rectification and control circuitry, leaving peak voltage and current of 90 V and 141 A, from which we infer an effective antenna impedance of 0.64 Ω. This is distributed between an antenna resistance of about 0.29 Ω, electrode resistance to seawater of about 0.05 Ω, about 0.1 Ω in wires and connectors, leaving about 0.2 Ω inferred to be the radiative impedance of the crust and seawater at the frequency of operation (about 8 Hz).

The total dipole moment is obtained by taking $2/\pi$ times the peak current to obtain 90 A for the effective amplitude of the waveform envelope (Figure 2a) and 71 A at each of the first and third harmonics as described above. The antenna was a 554-m length of 8.3-mm diameter insulated aluminum cable, so the dipole moment at each frequency was 3.9×10^4 Am. During operation the transformer package is towed behind the ship and kept a few meters off the seafloor by monitoring a free-running 12 kHz acoustic pinger mounted near the end of the wire. A combination of a 300-kg lead depressor weight above the transformer and a 100-kg steel bar on the first electrode (which is suspended 10 m below the transformer) ensured that the 15 m × 12 mm bronze electrodes were in contact with the seafloor most of the time.

The receivers must record very small seafloor electric fields autonomously during transmitter operation. These instruments are built around Onset Corporation's CPU88 computer and use the small computer systems interface to communicate with the mass storage device (Figure 3). Although the present configura-

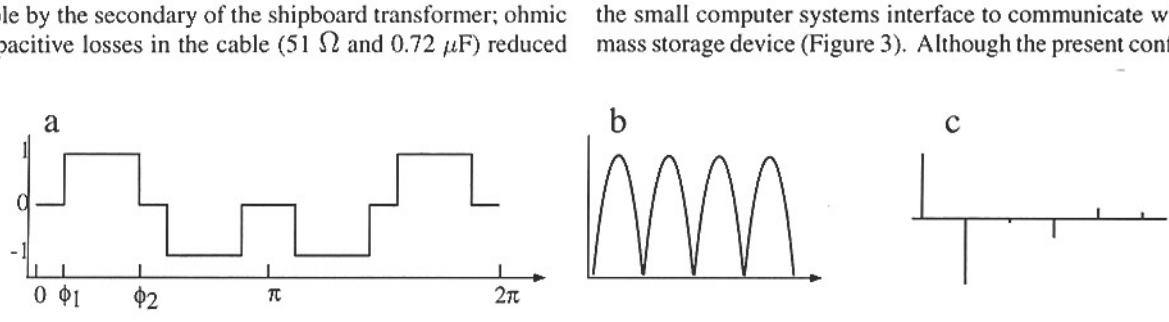

Figure 2. The waveforms generated by the controlled source. (a) The envelope of the waveform. (b) The form of the 120-Hz ripple on the low-frequency waveform shown in Figure 2a. (c) The odd harmonics generated when $\phi_1 = 22.0°$ and $\phi_2 = 83.5°$.

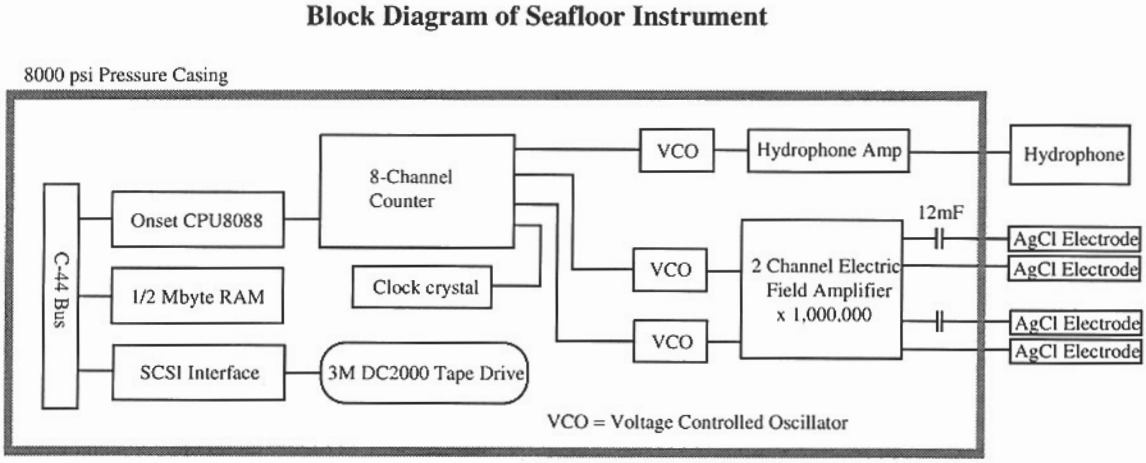

Figure 3. Block diagram of seafloor electric field recorders used in this experiment. The 16-bit, 8-channel counter in combination with the voltage controlled oscillators (VCOs) provides 16-bit analog to digital conversion. The 1/2 megabyte of random access memory (RAM) allows 15 min of continuous hydrophone and electric field recording at 2 Hz, as well as stacked electric field data sampled at 256 Hz, to be collected before the mass storage device needs to be powered and used.

tion uses a 250–500 Mbyte disk drive, during PEGASUS these drives were not available in appropriate physical size, power consumption, and price. Instead, we used 3M brand DC2000 tape drives with a formatted tape capacity of 40 Mbytes, necessitating synchronous stacking to compress the electric field data collected at a 256-Hz sampling rate. Electric field signals are passed through the ac-coupled, high-gain (10^6), low-noise amplifier described by *Webb et al.* [1985], and analog to digital conversion is carried out using voltage controlled oscillators (VCOs) and an eight-channel counter which also keeps count of time from an accurate crystal oscillator. The logger package can be configured as either a more modern version of the long-wire electromagnetic (EM) instrument (or LEM) described by *Webb et al.* [1985] or with a pair of semirigid, orthogonal 12-m-long antennas similar to our original electric field instrument (ELF) [*Young and Cox*, 1981]. The pressure case, plastic frame/protective cover, data logger, and twin 17-inch diameter glass flotation balls are common to both instruments. The ELF is quick to deploy and measures the full horizontal vector field but is restricted to ranges less than 10–20 km because of limited sensitivity due to short antennas (four 6-m-long plastic pipes terminated with 15-cm-long by 4-cm-diameter silver–silver chloride electrodes). With its much longer antenna terminated by 1-m-long electrodes, the LEM provides much greater sensitivity than the ELF. The LEM instruments are deep-towed to the seafloor and released in the manner described by *Webb et al.* [1985], ensuring the antenna cable (polyvinyl chloride insulated number 6 copper) is extended its full length behind the instrument on the seafloor. The electrodes closest to the instrument and steel anchor are positioned about 10 m away to reduce the effects of noise associated with electrolytic corrosion.

Figure 4 shows a map of the PEGASUS experiment. A total of 14 electric field receivers were deployed, of which 12 collected data, although of these one stopped recording before the start of transmission (George). Nine instruments were ELFs, deployed in a group close to the planned transmitter tow. Six of the ELF instruments collected good data during transmitter operation. Our previous experiment [*Cox et al.*, 1986] measured a very high resistivity for the oceanic lithosphere, and sensitivity studies [*Flosadottir and Constable*, this issue] show that to decouple the resistivity and thickness of this layer one needs very long ranges (100 km or more). Five LEMs were therefore deployed, four with 1000-m antennas and one (Quail) with a 3000-m antenna designed to extend source-receiver ranges out to 100 km or so. Each LEM had a secondary antenna one-third the length of the main antenna as a backup sensor. All LEMs collected data on the PEGASUS experiment.

The transmitter unit was towed behind the ship for about 28 hours at about 2.5 km/hour, but only the 13-hour section of the transmitter tow shown in Figure 4 was chosen for analysis. During that time the ship's heading and speed were nearly uniform, the transmitter antenna was in contact with the seafloor, and all receivers were close enough to recover a signal, with propagation both across and along the N–S tectonic fabric of the seafloor. Transmissions were in 15-min blocks at fundamental frequencies of 0.25, 1, 2, 4, and 8 Hz. Every second transmission was at 8 Hz (with 24-Hz overtone) because our sensitivity studies [*Flosadottir and Constable*, this issue] indicate the need for long-range data around 10 Hz. They also show that range has a larger effect on sensitivity than frequency, and indeed, we see little variation in electric field amplitude across the 2 orders of magnitude frequency range. Also, 8 Hz falls on a convenient part of the noise spectrum (see Figure 9 of *Flosadottir and Constable*), being a good compromise between contamination by magnetotelluric noise and loss of signal strength at high frequencies. Finally, previous experience had suggested that redundant data at a reference frequency would be useful for monitoring variations in conductivity near the transmitter.

Data Reduction

The raw data are 225-fold stacks of 4 s, 1024-point frames of data collected at 256-Hz sampling. Our transmissions at fundamental frequencies of 0.25, 1, 2, 4, and 8 Hz thus fall exactly in the Fourier bins for harmonics 1, 4, 8, 12, and 32, and similarly, the third harmonics of the transmission frequencies also fall on exact harmonics. There is therefore no side-lobe leakage at the transmission frequencies, and the initial data reduction consists of fast Fourier-transforming the unwindowed stacks (equivalent to performing a least squares fit to sinusoids of the bin frequen-

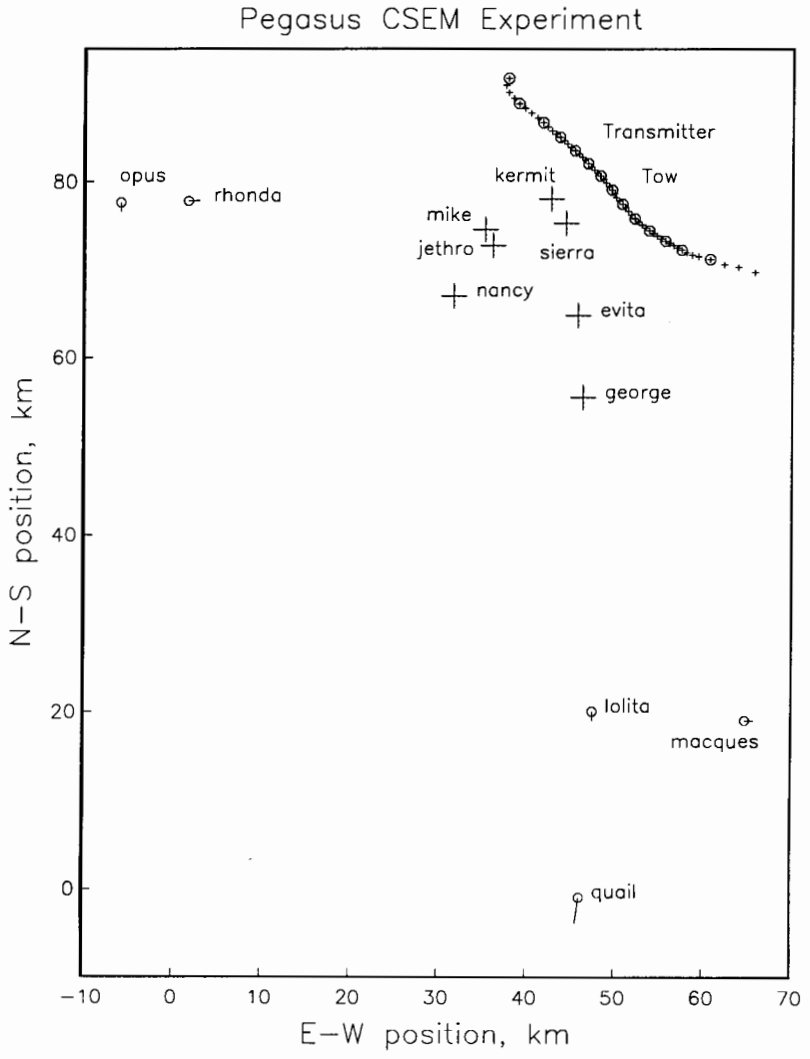

Figure 4. Map ot the experimental area (origin is at 34.5°N, 132.5°W). Of the instruments shown, only George failed to collect data during the transmitter tow. Plus symbols on the transmitter tow indicate position at the start of each 15-min stack, and open circle symbols represent hour marks. Electric field (ELF) instruments are shown as larger plus symbols, and open circle symbols with tails indicate postion, attitude, and actual scale length of long-wire electromagnetic (LEM) antennas.

cies). We use a fast Fourier transform (FFT) that is normalized to return a unit amplitude delta function from a unit amplitude sine wave, and all that remains to convert the data to electric fields is normalization by the stack fold, amplifier gains, VCO gains, and receiver antenna length. It is convenient also to divide by the source dipole moment to yield electric field per unit dipole, allowing direct comparison with modeling results.

In spite of the long antennas the signal to noise ratio on the LEMs was mediocre. Because relative range and azimuth vary little at the greater receiver distances (ranges for Quail varied between 76 and 97 km), we can synchronously stack data from most of the tow to reduce error. Examination of the phase data on the LEMs and other instruments shows that the transmitter time base was drifting -52 ms per hour relative to the receivers due to a technical problem of unknown cause. We have corrected the phases on the LEM data and synchronously stacked 11 hours of signal from most of the tow. We have also performed this integration on data from Nancy; although the range and azimuth change somewhat, this instrument is at the maximum range for an ELF to receive the signal, and without such processing the data are quite noisy.

Error analysis

Error estimation is a little more involved. We have the advantage that prior to the operation of the transmitter there is a considerable period of time during which the receivers make recordings of background noise. We exploit this and examine the statistics of 160 stacked electric field records on each channel of each instrument at each frequency made during this time. The normalized FFTs yield real (in-phase) and imaginary (out-of-phase) components of noise at signal frequencies. The Kolmogorov-Smirnoff (K-S) test for normality shows a surprising agreement with the ideal model of Gaussian noise, and more than 95% of the instrument/channel/frequency/component combinations pass the K-S test after trimming 1%-3% of the data on the tails of the distribution. All the data indicate equal variance for the two components. A few of the instruments show significantly nonzero means for the real component only. One must conclude that this reflects an instrumental source of noise, although we do not understand the mechanism. However, the effect is very small and has little impact on our analysis. Given equal variance for the two components, an average is made of the standard errors in the real and imaginary terms. Errors thus

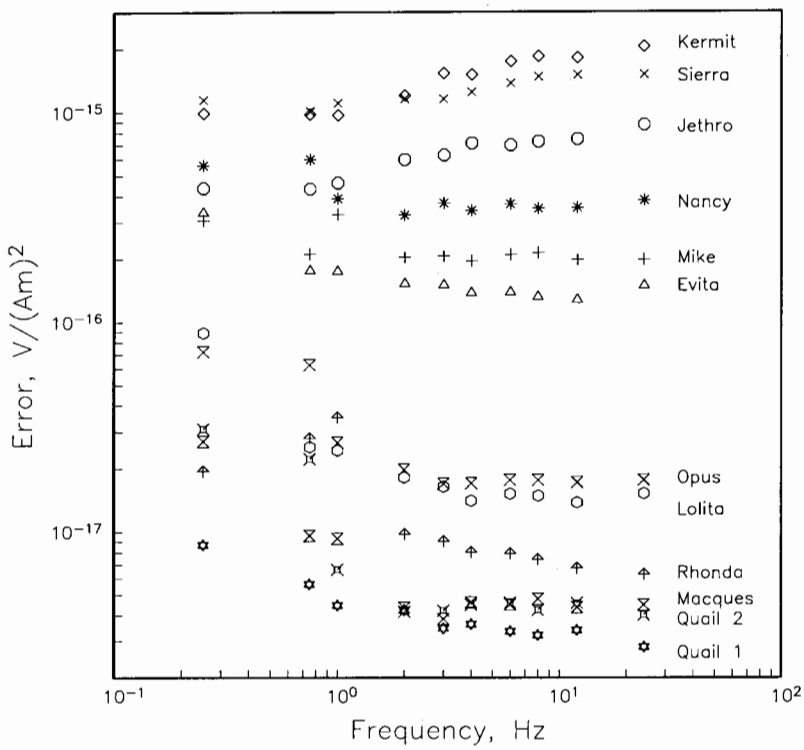

Figure 5. Errors at transmission frequencies for all instruments, normalized by antenna length and source dipole moment. ELFs have a higher noise threshold than LEMs, but within the ELFs the instruments fall into two groups (Kermit/Sierra/Jethro and Nancy/Mike/Evita) having slightly different wiring configuration. With a 3 km antenna, LEM Quail has the lowest noise threshold, about 10 picovolts/meter after the source dipole moment is removed.

obtained for the entire instrument suite are shown in Figure 5. Noise arises from electrodes, water and ground motion, geomagnetic variations, and instrumental sources. The different sensitivities of the ELFs and LEMs is clear, with the noise levels for the ELFs being 1 to 2 orders of magnitude higher than for the LEMs (recall that the noise signal has been divided by antenna length). The high frequency noise for Kermit, Sierra, and Jethro is probably instrumental, as the spectrum is blue and the two channels (only channel 1 shown here) produce similar noise estimates. The most likely source of instrumental noise is the tape recorder, which is running during the first few stack frames; recent experiments using disk drives have not required stacking, and the detrimental effect of operating the mass storage device during data collection has become apparent. These three noisy ELFs were all configured slightly differently from Nancy, Mike, and Evita, but it is unclear why the two classes of instrument are different. The tape drives are actually closer to the e-field amplifiers in the quiet instruments, but the ground circuitry is wired slightly differently and possibly better. The LEMs are all configured the same way as the noisy ELFs, and at high frequency we see that on average the noise levels are simply the inverse of antenna length, with Quail channel 1 being 3 times quieter than the other LEMs and these 100 times quieter than the noisy ELFs. At low frequencies the ELFs converge, probably dominated by electrode noise, and the noise in the LEMs increases, perhaps due to electrode noise but also likely caused by magnetotelluric noise finally leaking through the overlying ocean and from microseismic motion [*Webb and Constable*, 1986].

We prefer to interpret the amplitudes of the electric fields rather than the individual components or phases because, to obtain a phase estimate with a 10% error at 24 Hz, one must have the relative timing of the transmitter and receiver accurate to 0.7 ms over the 20-day experiment (1 part in 2×10^9). This is beyond the capabilities of our instruments. Synchronous stacking, on the other hand, relies on timing being maintained only over the 15 min duration of the stacking period, or a clock accuracy of 1 part in 10^6. This is well within the capabilities of the instruments, so amplitudes are faithfully recorded. It is possible that relative phase between the first and third harmonics could be exploited, but *Flosadottir and Constable* [this issue] demonstrated that, for 1-D structures at least, phase is not likely to improve resolution.

Amplitudes are not normally distributed but are distributed as Chi-squared with 2 degrees of freedom if the two components are normally distributed. When the component distributions are zero-mean, the difference between χ_2^2 and a normal distribution is significant (e.g., χ^2 cannot be negative while half the zero-mean normal distribution is). However, we are interested in estimating errors for nonzero signals whose effect is to displace the means of the signal plus noise away from the origin. Thus we are dealing not with a central χ_2^2 distribution but a noncentral one, and as long as the signal to noise ratio is about 3 or more and the component noise distributions have equal variance, we can use the standard deviations of the components as normally distributed errors on the data.

For the LEMs, with a single component of the electric field available, these amplitudes and errors are the basic data for interpretation. The usual parameters associated with dipole transmission (frequency, range, and azimuth) need to be augmented with the relative orientation of the receiver antenna, which we term rotation (see Figure 6). The ELFs, however, provide two orthog-

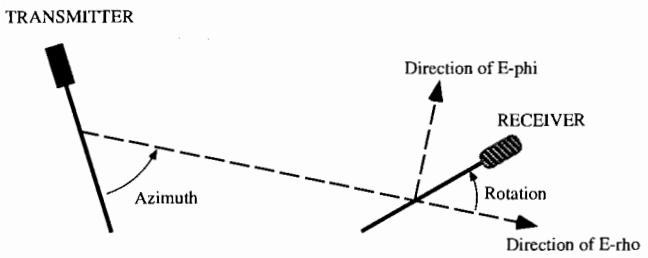

Figure 6. The geometry associated with a transmission to a LEM receiver. A line from the center of the transmission antenna to the center of the receiver antenna defines the radial, or e-rho, component of the electric field. At 90° to this (anticlockwise) is the tangential, or e-phi, component. We define the azimuthal angle as the angle between the trailing end of the transmitter antenna and the e-rho direction, measured anticlockwise. These are all features normally associated with a dipole field. We must add another angle, the rotation, to describe the angle between the e-rho direction and the instrument end of the receiver, measured anticlockwise.

onal components of the electric field, and while each channel can be treated independently as in the LEM instruments, we can combine the two channels in a polarization ellipse to simplify the geometry associated with the experiment.

Polarization Ellipses

Grant and West [1965, pp. 482-484] describe the concepts behind the polarization ellipse. On each (orthogonal) axis of an ELF we record the time-varying electric field in that direction. We describe the electric field for each axis in terms of complex numbers (a_1, b_1) and (a_2, b_2) (the subscript refers to the channel or axis). We can convert these into amplitude and phase:

$$E_i = |(a_i, b_i)| = \sqrt{a_i^2 + b_i^2} \tag{3}$$

$$\phi_i = \arctan(b_i/a_i) \tag{4}$$

respectively, where arctan() is assumed to preserve the quadrant of ϕ. As from *Smith and Ward* [1974], the tilt angle α and two axes of the polarization ellipse P_1 and P_2 are then given by

$$\tan 2\alpha = \frac{2(E_2/E_1)\cos(\phi_2 - \phi_1)}{1 - (E_2/E_1)^2} \tag{5}$$

$$P_1 = |E_2 e^{i(\phi_2 - \phi_2)} \sin\alpha + E_1 \cos\alpha| \tag{6}$$

$$P_2 = |E_2 e^{i(\phi_2 - \phi_2)} \cos\alpha - E_1 \sin\alpha| \tag{7}$$

if we assume that channels 1 and 2 form a right-handed system. Note that while we have stated that phase is too inaccurate for interpretation, the relative phase of the two channels used in this calculation has an accuracy limited only by the signal to noise ratio. Note also, however, that in order to avoid 180° errors in the relative phase the polarity of the two channels must be known and taken into consideration. The tilt angle α is an anticlockwise rotation of P_1 from the positive axis of channel 1. In order to plot the polarization ellipses, the orientation of the instrument must be added to α. An example of the polarization ellipses for all ELFs during an 8 Hz transmission is shown in Figure 7.

The computation and display of the polarization ellipses has several advantages. By incorporating the fields of both channels, four independent numbers a_1, b_1, a_2, b_2 are reduced to one, and the rotation is removed to leave only frequency, range, and azimuth as experimental parameters. Although the orientation of the ellipse axis is a weak function of conductivity structure, the orientation of the receivers and particularly the transmitter are subject to uncertainty. The major axis of an ellipse $\max(P_1, P_2)$ is a more robust estimation of the electric field magnitude, independent of receiver orientation and relatively insensitive to transmitter azimuth.

Data

We concentrate our analysis on the 8-Hz data. As described above, half the data were at this frequency, and the third harmonic, 24 Hz, was below the noise threshold at ranges greater than 20 km. Figure 8 shows magnitude of polarization ellipses (for ELFs) and electric field amplitude (for LEMs) at 8 Hz as a function of range and instrument. We see the approximately r^{-3} amplitude dependence expected for a dipole source. The internal consistency of the data is extremely good considering the technical difficulty of the experiment. We do not see the large sample to sample scatter reported by *Evans et al.* [1991] for a mid-ocean ridge experiment and attributed to small-scale heterogeneity in near-surface structure. The systematic interinstrument variation between Kermit and Sierra at short ranges is probably due to a 500 m or so cumulative error in navigation of the transmitter and receivers. Some interinstrument variation is due to changing azimuth and is why Evita and Jethro have higher amplitudes at 13-km range than do Sierra and Kermit. Finally, some of the variation in the data could be due to the effects of topography or electrical anisotropy of the crust or mantle, which will be addressed in another paper. The lower scatter for this experiment, compared with the ridge axis data, is understandable in terms of the moderately uniform, thin blanket of sediment and a diagenetic loss of extreme porosity structure

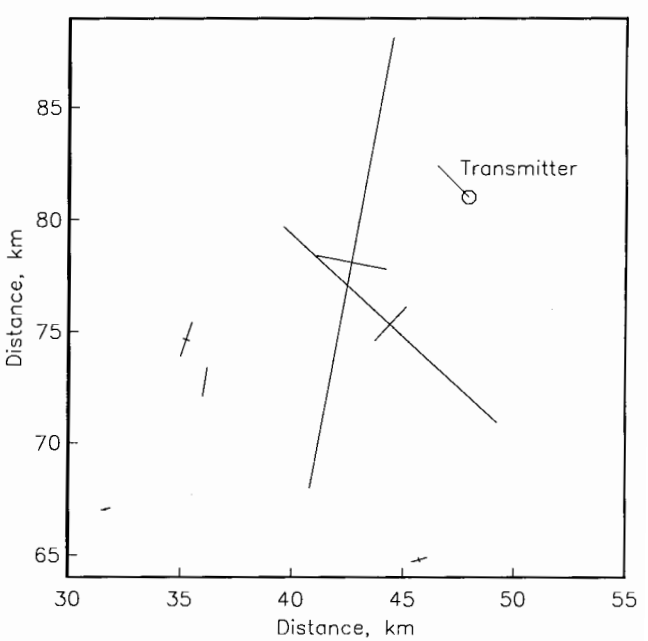

Figure 7. Polarization ellipses recorded by all ELFs for one 8-Hz transmission. Scaled amplitudes and directions of the major and minor axes of the ellipses are plotted.

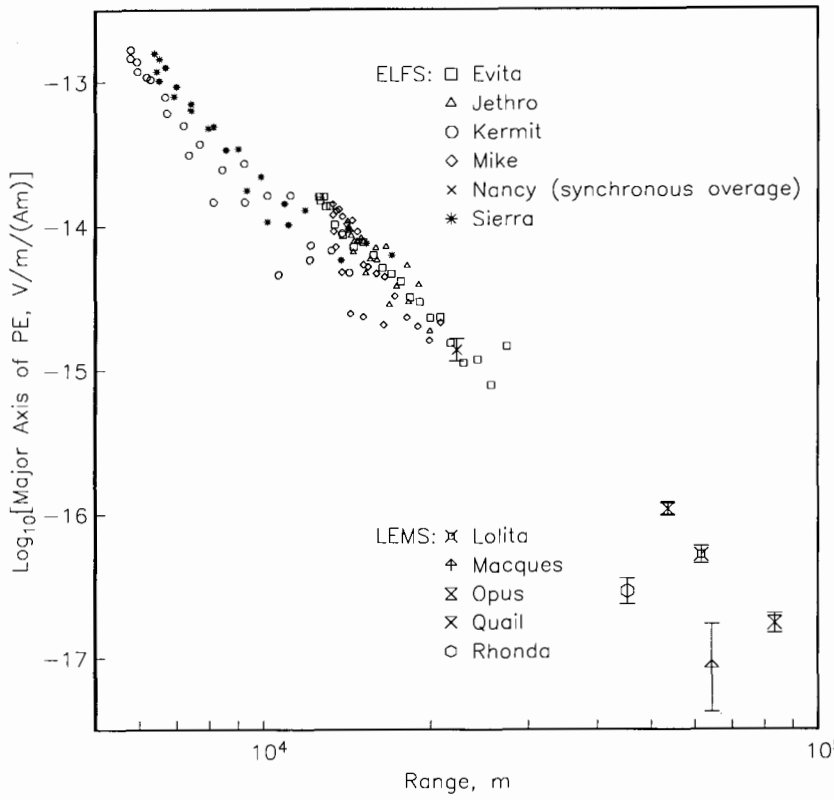

Figure 8. All data collected at 8 Hz during this experiment, expressed as electric field magnitude for LEMs and amplitude of the polarization ellipse major axis for ELFs.

in the older crust. At ranges of 5 to 10 km, where there is overlap with the ridge data set of *Evans et al.* [1991], the PEGASUS data are systematically over half an order of magnitude larger in amplitude, indicating lower electrical conductivities at the older site.

Modeling

We use the 1-D forward routine of *Chave and Cox* [1982] as the kernel of the regularized inversion scheme of *Constable et al.* [1987]. The large number of unique ranges makes the forward and inverse problem computationally demanding, and *Evans et al.* [1991] averaged the data in range bins to reduce the effects of scatter and to make the data set more compact. They could accomplish the averaging without distorting the data set because the azimuth did not vary significantly during the ridge experiment. However, in this study the azimuth for the nearer instruments varied by more than 200°, and we need to model the data points individually.

Flosadottir and Constable [this issue] explain how to manage the larger data set in a computationally efficient way and how to implement the "Occam" inversion scheme described by *Constable et al.* [1987], which generates smooth models of resistivity as a function of depth. This is an effective, stable, and often geologically realistic way to interpret the data, but relies on a reasonable a priori estimate of data error, because large resistivity contrasts appear in the model when one attempts to overfit the data. As explained in the original paper [*Constable et al.*, 1987], if the data errors are known and Gaussian and the model space adequate, the expected misfit has a root-mean-square error of 1.0. *Smith and Booker* [1988] offer the more conservative approach of taking the 95th percentile of the χ^2 distribution. However, both approaches assume one has a good estimate of data error. For the seafloor data the measurement error is often very small and takes no account of systematic errors in navigation or effects caused by non-1-D structure. The bin averaging carried out by *Evans et al.* [1991] allowed such errors to be estimated from the statistics of the scatter and produced self-consistent errors that allowed the data to be fit to RMS 1.0 with some confidence. The more complicated geometry of our experiment makes it difficult to average in this way.

We present another technique for estimating an appropriate misfit level based on the requirement that residuals be random as well as of acceptable size. If a large misfit is requested in the smooth inversion, residuals will tend to be distributed in a non-random way, usually with bias at short and long ranges because an overly smooth model fails to achieve adequate structure in the shallow and deep parts of the model. As we decrease the required misfit, this range-dependent structure in the weighted residuals disappears. This is somewhat similar reasoning to that of *Smith and Booker* [1988], who argued that the model norm (roughness criteria) should be modified to ensure no structure in the residuals of magnetotelluric data. We have inverted this argument; putting our faith in the appropriateness of the model norm (logarithmic resistivity versus logarithmic depth), we use serial correlation in the data residuals as part of the misfit criterion.

This process is probably best illustrated with the actual data. Initial modeling suggests that the data can be fit with an average error of about 30% with a simple 1-D model. Errors for four data (out of 120) with residuals greater than 3 standard errors were increased to 60% to avoid bias by these few points. Figure 9 shows weighted residuals versus range and misfit level, and

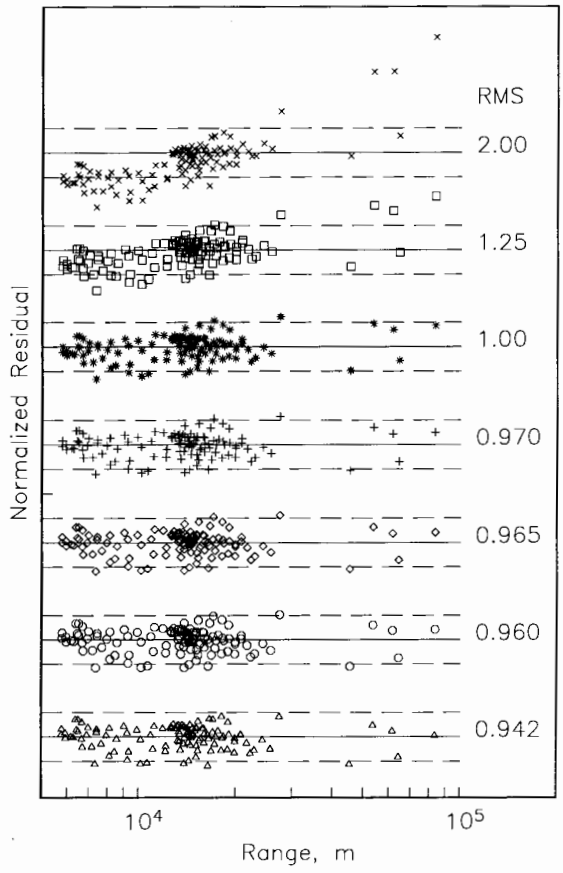

Figure 9. Residuals as a function of total data misfit (expressed as root-mean-square of normalized residuals). Corresponding models are shown in Figure 10a. For each fit the solid horizontal line denotes zero and the broken lines are at plus and minus 2 standard errors. The slope is pronounced at high misfits, disappearing around RMS 1.00 and statistically insignificant below RMS 0.970. The least squares slope actually changes sign to negative at RMS 0.960.

Figure 10a shows the corresponding models. It is clear that data for fits of RMS 2.00 and 1.25 are overestimated at short range and underestimated at long range. We can quantify the degree of bias in the residuals to first order by fitting a least squares line though them. When the slope of the line is no longer significantly different from zero, we no longer have a biased fit. In this case this occurs at RMS 0.970; at 0.960 the slope changes sign from positive to negative. There is a slight negative bias remaining in the residuals at a range of 10 km, but we cannot remove this by decreasing misfit. We can use these results to choose RMS 0.970 as a conservative misfit level, deeming larger misfits as unacceptably tolerant and smaller misfits as unacceptably extreme.

The models associated with the different levels of misfit (Figure 10a) are surprisingly similar, with the main difference being behavior shallower than 1-km depth. In this region we see resistivities varying between 0.01 Ω m and 100 Ω m. We know from borehole studies [*Becker et al.*, 1982] that resistivities are about 10 Ω m above a depth of about 500 m, corresponding to a misfit of around 1.00. All models exhibit a sharp increase in resistivity starting at a depth of 400 m, persisting until resistivities of 10^4 – 10^5 Ω m are attained at depths of about 20 km. Terminating resistivity (below 100 km) is remarkably tolerant to misfit level, varying only between 10,000 Ω m and 50,000 Ω m. We will use further constraints on the modeling to examine shallow and deep structure.

Two-layer Models

The smooth inversion scheme allows the roughness penalty to be relaxed at given depths to allow unpenalized discontinuities to develop [see, e.g., *deGroot-Hedlin and Constable*, 1993; *Constable*, 1993]. If we do this systematically (Figure 10b), we find that, for depths 1400 m or shallower, no structure other than two simple layers is required using our conservative misfit level of 0.970. When the discontinuity is placed deeper than 1400 m, structure develops above and below the conductivity jump, allowing us to infer that a drop in conductivity is required somewhere in the upper 1400 m of the section.

It appears that the upper, conductive layer can be made arbitrarily thin and that as thickness is decreased conductivity increases. In dc resistivity sounding this would be termed S-equivalence, and we would expect that the conductivity-thickness product would be invariant. This is not the case here, but rather, to a first approximation, the square root of conductivity times thickness ($T\sqrt{\sigma}$) is preserved. This corresponds to constant attenuation through this layer, as the signal path can be considered to propagate down from the transmitter to the resistive layer, along the resistive layer and then propagate up through the upper layer again to the receiver, much like seismic refraction (and discussed in detail by *Flosadottir and Constable*, [this issue]). This vertical propagation is somewhat similar to that of the magnetotelluric method, where layers may also be characterized by $T\sqrt{\sigma}$ [*Larsen*, 1981]. The average value of $T\sqrt{\sigma}$ is 187 $\sqrt{\text{Sm}}$, which corresponds to about 1 skin depth at 8 Hz for all the layers. (In our modeling it is actually $T\sigma^{0.64}$ that is invariant; the difference between this and $T\sqrt{\sigma}$ can be attributed to the increased difficulty in fitting the simple model as the layer boundary approaches 1500 m.) Because we do not have data at ranges comparable to the thickness of the conductive layer (our shortest range is a little less than 6 km), we cannot constrain the conductivity separately from thickness. Data from an earlier experiment on younger, 25 Ma crust [*Cox et al.*, 1986] were modeled as two layers with the upper layer 1000 Ω m and 5 km, or $T\sqrt{\sigma}$ equal to 160 $\sqrt{\text{Sm}}$. This is comparable to the present result, but with a shortest source-receiver range of 13 km the older experiment was not able to constrain the conductivity increase to occur shallower than 5 km.

Of course, we can set a lower limit on the thickness of the conductive layer using the physical constraint that the uppermost layer is unlikely to be more conductive than seawater. This corresponds to the most conductive model plotted in Figure 10b, with a thickness of 68 m. For the 2-layer models the resistivity of the deeper layer is again almost invariant, suggesting that propagation between source and receiver provides a unique determination of this resistivity. At 8 Hz the skin depth in the basement is 25 km, and so the ranges available in this experiment can constrain the resistivity of this layer (at a range of 50 km, attenuation in the resistive layer equals that in the uppermost layer).

Maximum Depth of Inference

In Figure 10a, we see the RMS 0.942 model with conductivity structure at a depth of 60–100 km. We might consider this the depth to which we may infer conductivity structure; after all, our source-receiver separation extends to this distance. The size

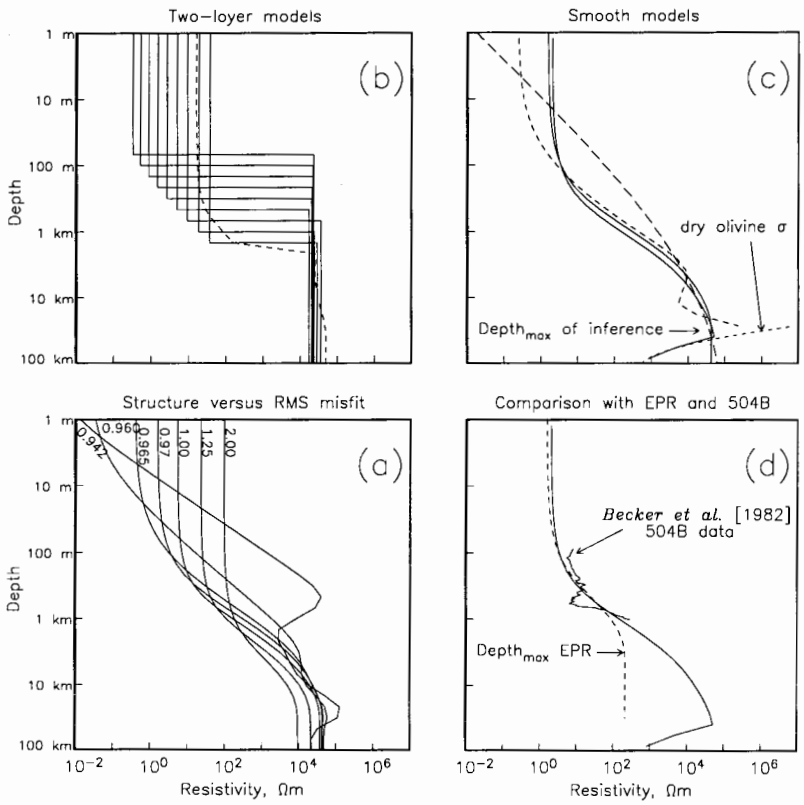

Figure 10. Exploring model space. (a) Smooth (in a first-derivative sense) models as a function of total misfit are shown. Residuals for these models are shown in Figure 9. We choose RMS 0.970 as the appropriate misfit and all other models shown in Figure 10 achieve that level of fit. (b) Two-layer models generated by relaxing the roughness penalty at various depths are shown. This generates a suite of models having an upper layer approximately one skin depth thick. (c) Favorite models, with maximum smoothness in a first derivative (solid lines) and second derivative (long-dashed line) sense are shown. The curve marked "dry olivine" is a laboratory-derived model of olivine conductivity, and one inversion has been constrained to follow this (second solid line). The short-dashed curve is a model with extremely high conductivity below 30 km. If the high conductivity is forced any shallower, no models can be found with acceptable fits to the data, and so this indicates the maximum depth of inference. Below this depth any conductivity can be accommodated by adjusting shallower structure. (d) Comparison of the olivine-constrained model (solid line) with model from the East Pacific Rise (EPR) (dashed line), obtained by treating the EPR data of *Evans et al.* [1991] in the same manner as the PEGASUS data. Again, a maximum depth of inference has been obtained. Also shown is the borehole log of *Becker et al.* [1982].

of the resolving kernels could be quantified using, for example, the traditional experimental design approach of *Glenn and Ward* [1976], in which a linearized sensitivity analysis is performed around a parameterized model. However, although the resolving kernels for electromagnetic methods have very long tails, in this case extending past 100-km depth for homogeneous structure, they are very model dependent (see, for example, models R and C of *Flosadottir and Constable* [this issue]), and any linearized analysis is valid only close to the assumed structure. This tends to overestimate the maximum depth of resolution.

Parker and Whaler [1981] offer us an approach to determine the maximum depth of inference, rather than merely resolution. Assuming one has the machinery to obtain a least squares solution, if the model is forced to contain an infinite conductor or insulator at a given depth and the ensuing least squares misfit for such a terminated model is within the tolerated misfit, then clearly one can say nothing about the conductivity below the depth of the conductor or insulator.

Parker and Whaler [1981], indeed, had a rigorous least squares solution to the 1-D magnetotelluric (MT) problem considered, comprised of a set of delta functions in conductivity. We do not have a rigorous result for the marine EM problem, but *Heinson and Constable* [1992] showed that the Occam process is quite efficient at approaching the least squares solution, at least for 1-D MT. The appearance of large oscillations in conductivity in Figure 10a suggest that this is also the case here. If we assume this is so, and terminate our models with extremely conductive (10^6 S/m) or extremely resistive (10^{10} Ω m) basement at increasingly shallow depths, we can discover at which depth we are no longer able to compensate for the terminating structure by altering shallower structure. We find that placing an extreme conductor shallower than 30 km deep prevents us from being able to fit the data to our accepted level of RMS 0.970. Extreme resistive structure provides a weaker constraint on depth of inference, with a depth of less than 68 km intolerable. We interpret this to indicate that below 68 km we can say nothing about conductivity structure at all, between 30 and 68 km we can merely bound the maximum value of resistivity, but above 30 km we are able to discern details of the actual conductivity profile.

This is a powerful and important result. First, 30–60 km are considerable depths, well into the upper mantle. Second, we have demonstrated an intrinsic depth resolution for the seafloor controlled-source EM method. One might have thought this to be expected, but *Parker* [1984] showed that for 1-D resistivity sounding on land an arbitrarily thin model fits the data as well as any other, no matter what the source-receiver offset. We have shown above that there is no intrinsic resolution to the thickness of the upper conductive layer, so it is gratifying that the minimum thickness of the resistive layer is constrained.

Smooth Models

Figure 10c shows models that are maximally smooth in both a first- and second-derivative sense, and which fit the data to our tolerated misfit. Models smoothed with a first-derivative penalty tend to be "flat" wherever possible, and models smoothed using a second-derivative penalty prefer structure with a constant slope (which need not be zero). We see that the second derivative model takes advantage of the ambiguity in shallow structure to construct an uppermost region of constant slope but that deep resistivity cannot be made arbitrarily high, necessitating a change of slope to accommodate a terminating resistivity of about $7 \times 10^4\ \Omega$ m.

Cox et al. [1986] pointed out that models terminating in deep resistive structure are unrealistic, because we know both from magnetotelluric sounding and the conductivity behavior of minerals at high temperature that conductivity must increase at depth. Following their example, we constrain the deep structure to follow the expected conductivity of olivine-rich rock along the geothermal gradient. Specifically, we use the SO2 olivine conductivity model of *Constable et al.* [1992] and the geothermal model for 40 Ma lithosphere described by *Heinson and Constable* [1992]. This does not have a profound effect on our models; the olivine conductivity curve intersects the terminating resistivity just below the maximum depth of inference and so is easily accommodated by a smooth model fitting to RMS 0.97. We have considered only the total misfit in these models; it is perhaps worth noting that the models terminating in more conductive structure fit the LEM data at ranges greater than 60 km slightly better than for smoother models.

Cox et al. [1986] suggested that the marine EM method is preferentially sensitive to the resistivity-thickness product (transverse resistance) of the lithosphere. Of the models presented here the one with the smallest transverse resistance is the one constrained by olivine conductivity, in which $\rho T = 1.7 \times 10^9\ \Omega\ \text{m}^2$. For the depth of inference model, $\rho T = 2.5 \times 10^9\ \Omega\ \text{m}^2$. For all other models which terminate in a resistive half-space, ρT is, of course, arbitrarily large. It appears that a reasonable lower bound on the transverse resistance of the lithosphere is about $10^9\ \Omega\ \text{m}^2$; *Constable* [1990] came to a similar conclusion after discussing a variety of experiments and noted the importance of this parameter on both oceanic induction studies and marine magnetotelluric sounding.

Flosadottir and Constable [this issue] considered the problem of estimating the thickness of the lithospheric resistor and the conductivity of the underlying asthenosphere, using the controlled-source method described here. They show that with sufficient data at ranges of about 100 km at a frequency around 10 Hz these features are indeed resolvable. However, our one data point at 85 km is inadequate to distinguish the two models considered in the companion paper. Both models fit our data equally well overall, with model R very similar to the model in Figure 10d (because both models were constrained a priori to follow the olivine electrogeotherm) and model C fitting the longest range datum slightly better.

Comparison with Other Studies

There are extremely few estimates of lithospheric resistivity for the seafloor. The experiment of *Cox et al.* [1986] was more limited than PEGASUS; there was a smaller selection of source-receiver ranges and computational capabilities at that time restricted modeling to only a few layers. The earlier experiment lacked resolution in the crust because no data were collected at ranges shorter than 13 km, but the lithospheric transverse resistance was estimated to be almost identical to that here. Even so, the actual resistivity of the upper mantle is better estimated by PEGASUS, with ranges up to 97 km compared with 60 km. Neglecting pathological models associated with our depth of inference study, the acceptable range of lithospheric resistivities in our models is 2 to $7 \times 10^4 \Omega$ m.

A controlled-source experiment on the East Pacific Rise (EPR) at 13°N was conducted using almost identical techniques to those here [*Evans et al.*, 1991, 1994]. The data extended to shorter maximum ranges because only ELF instruments were available, but in the region of overlap (5–10 km) the EPR electric field amplitudes are almost an order of magnitude smaller than for PEGASUS. In order to make a direct comparison of the two experiments, we reprocessed the EPR data in the same manner as discussed here. We went back to the original data collected by Scripps ELFs and shown in Figure 4 of *Flosadottir and Constable* [this issue]. We again chose a misfit level based on structure in residuals and estimated a maximum depth of inference (3200 m) based on inclusion of highly conductive basement. The resulting first-derivative smooth model is plotted in Figure 10d.

Surface structure, above about 1 km depth, is almost identical for the two models. Given the nonuniqueness associated with surface conductivities, this result is probably fortuitous, but we can infer that the integrated conductivity of the surface layer is similar for the two regions. Also shown in Figure 10d is the borehole log of *Becker et al.* [1982] from deep sea drilling project (DSDP) hole 504B, in 6 Ma crust off Costa Rica (the data have been shifted to replace the 270 m of sediments at DSDP hole 504B with the 35-m average of the PEGASUS site). Our inversions agree well with the borehole log and suggest that the steepest rise in resistivity occurs 600–800 m deep, approximately coincident with the dike-gabbro boundary in the crust.

Although the surface conductivity of the three experiments (EPR at 0 Ma, 504B at 6 Ma, and PEGASUS at 40 Ma) seems to be similar, the PEGASUS inversions require conductivities an order of magnitude lower than the EPR at depths of 2–3 km. While the low geothermal gradient and ophiolite studies, which indicate water pentration at least as deep as the mantle, suggest that the crust under the PEGASUS experiment is in a cold wet rock regime, the terminating conductivity in the EPR inversions is consistent with olivine rock just below the solidus (1300° or so). That a more highly conductive layer, characteristic of partially or fully molten rock, cannot easily be incorporated into the EPR models at depths shallower than 3 km supports the conclusion of *Evans et al.* [1994] that a well-developed magma chamber was not indicated by the electrical experiment. The recent paper by *Unsworth and Oldenburg* [1995] shows that, given adequate data, the experiment can well resolve such a feature, even when it is of limited lateral extent.

As mentioned above, marine MT soundings are sensitive to the increase in conductivity at 50–100 km thought to be as-

sociated with solid state conduction in hot olivine-rich rocks. Although many of the MT models [e.g. *Filloux*, 1980; *Oldenburg et al.*, 1984] feature resistivities of 100–1000 Ω m in the uppermost 30 km, this region is not well resolved by the MT experiments. The much higher resistivities in our models are easily compatible with the MT results for one-dimensional (1-D) modeling.

Discussion and Conclusions

At temperatures below about 1000°C neither olivine nor any common rock-forming mineral is likely to be a major contributor to rock conductivity. The PEGASUS model of Figure 10d intersects the olivine electrogeotherm at a depth of 40 km and at a temperature of 800°C. Below this depth our data are compatible with a hot, dry rock regime, but our maximum resistivity of 7×10^4 Ω m requires that shallower than about 40 km, conductivity must be dominated by trace materials on grain boundaries. At crustal depths this is probably water. The relationship between porosity ϕ and electrical resistivity ρ is traditionally described by Archie's law: $\rho_{\text{bulk}} = \rho_{\text{pore fluid}}\phi^{-m}$ where the resitivity of the minerals is considered much larger than the bulk resistivity. Work by *Pezard* [1990] and *Evans* [1994] suggests that the exponent m is close to 1 in surface submarine basalts, implying an efficient reduction in resistivity by a connected network of water-filled cracks. Using this exponent and cool seawater conductivity (3 S/m), porosity is inferred to be about 10% at 100 m depth, decreasing to 0.1% at 1 km depth in the gabbros. However, the classic paper by *Brace and Orange* [1968] demonstrated that for a broad suite of crystalline rocks, in which gabbros and peridotites were well-represented but extrusives were absent, the traditional exponent of $m = 2$ held to very low porosities (0.1%). The resistivity between 1 km deep and the moho can be well modeled using a uniform layer of 3×10^4 Ω m and using a hot seawater conductivity of 5.2 S/m (after *Cox et al.* [1986], who extrapolated data from *Quist and Marshall* [1968]); we obtain a volume fraction of water of 0.3%.

Water is not the only trace material that can enhance conduction and, indeed, presents a problem in the coolest part of the upper mantle where one assumes it will combine with olivine to form serpentine and magnetite. *Stesky and Brace* [1973] examined the electrical conductivity of serpentinized rocks with the specific goal of understanding the results from early oceanic electrical experiments. Magnetite, forming connected networks around relic olivine grains, lowered resistivity dramatically in some of their rocks to below 1000 Ω m in cold, dry samples. However, for most samples conductivity was well explained by porosity, water, and Archie's law with an exponent of 2. If the more conductive rocks are characteristic of in situ serpentization of oceanic upper mantle, we can easily rule out such alteration below depths of 1400 m, based on the low conductivities required by our data, but serpentinization producing a poorly connected and so less conductive magnetite phase would indeed be possible. *Constable and Heinson* [1993] discuss other possible candidates for enhancement of mantle conductivity and deliver arguments against their contribution to a deeper high-conductivity zone in the mantle. However, the much higher resistivity of the uppermost mantle could well be limited by traces of hydrogen or carbon or by solid state properties of olivine associated with straining, grain boundaries, or oxygen fugacity.

We have noted that high lithospheric resistivities have little effect on a one-dimensional MT sounding, but the large transverse resistance of the uppermost mantle and lower crust has a considerable impact on 2-D and 3-D magnetotelluric models which feature the electrical boundary represented by the coastlines [*Heinson and Constable*, 1992]. This feature has a profound effect on induction in the ocean by natural magnetic fields, especially near passive continental margins, although subduction and spreading centers may lower the high resistivity locally [*Tarits et al.*, 1993]. The magnitude of the effect was quantified in a simple way by *Cox* [1980], who defined a compensation length $L = \sqrt{ST}$ in which S is the longitudinal conductance of the ocean (conductivity times thickness) and T is the transverse resistance of the seafloor. Horizontal distances of order L are required before charges built up on coastlines as a result of induction by natural fields can leak into the conductive parts of the mantle. This is, in essence, the oceanic side of the well-known coast effect in geomagnetic induction. However, while the continental side of the coast effect, manifest in the vertical magnetic field, decays with scale lengths of hundreds of kilometers, the transverse electric field decays on the oceanic side over $L = \sqrt{3\ \text{S/m} \times 4000\ \text{m} \times 10^9 \Omega\text{m}^2} = 3500$ km. As *Heinson and Constable* [1992] show, the pervasive coast effect needs to be considered when interpreting marine MT results. However, low leakage of electric fields from the ocean into the lithosphere is beneficial to the measurement of barotropic water flow through the use of seafloor electric field sensors [e.g., *Filloux*, 1987; *Luther et al.*, 1991].

In conclusion, a seafloor controlled-source electromagnetic experiment can be used to replace the high-frequency electromagnetic energy lost from the magnetotelluric field by attenuation in the conductive seawater layer. By designing a transmitter to maximize the current injected into the seawater, building electric field receivers with kilometer-scale antennas, and integrating signals for 15 min to 12 hours, source-receiver separations up to 97 km have been achieved on 40 Ma normal oceanic lithosphere. We have shown that this gives our electrical experiment a maximum depth of inference of 30 km, with bounds on conductivity to depths of 60 km. Resistivity is about 10 Ω m near the surface, rising rapidly at a depth of 500–1000 m and achieving 2–7 $\times 10^4$ Ω m in the upper mantle. We can place a lower bound of 10^9 Ω m^2 on the transverse resistance of normal oceanic lithosphere. An estimated 10% porosity in the extrusives and sediments shallower than about 600 m appears similar to studies conducted on younger lithosphere of 0 and 6 Ma. Below the extrusives, porosity drops dramatically to an estimated 0.1% to 0.3%. Some enhancement of dry olivine conductivity is required in the uppermost mantle, but below 40 km our data are compatible with a dry olivine electrogeotherm having a resistivity, temperature, and depth triplet of 50000 Ω m, 850°C, and 40 km, respectively.

Acknowledgments. Numerous people have contributed to this study, which is the product of many years spent developing instruments, techniques, theory, and computer code. The captains, crews, and technicians of the Research Vessels *New Horizon*, *Ellen B. Scripps*, *Robert Gorden Sproul*, and *Charles Darwin* have played an essential role in our work; a cruise on the *New Horizon* collected the PEGASUS data set with financial support from the National Science Foundation. Technical help from Tom Deaton and Jacques Lemire supported instrument development, construction, and preparation. We thank John Hildebrand and Mark Zumberge for providing bathymetry and sediment thickness data for the "big G" site, Walter Anderson for his fast Hankel transform code, Alan Chave for providing his 1-D forward modeling code, and Agusta Flosadottir for implementing derivative calculations in this code and suggesting changes in this paper. The EPR data set was collected in collaboration with Martin Sinha, Martyn Unsworth, and Robert Evans of Cambridge University. Bob Parker is thanked for much help over the years and the code PLOTXY, which was used for many of the fig-

ures in this paper. Finally, but certainly not least, a long and excellent collaboration with Spahr Webb has benefited our work tremendously, especially the extensive PEGASUS experiment described, in part, here. Helpful reviews by M. Zhdanov and P. Wannamaker led to an improved manuscript.

References

Becker, K., et. al., In situ electrical resistivity and bulk porosity of the oceanic crust Costa Rica Rift, *Nature, 300*, 594–598, 1982.

Brace, W.F., and A.S. Orange, Further studies of the effects of pressure on electrical resistivity of rocks, *J. Geophys. Res., 73*, 5407–5420, 1968.

Chave, A.D., and C.S. Cox, Controlled electromagnetic sources for measuring electrical conductivity beneath the oceans,1, forward problem and model study, *J. Geophys. Res., 87*, 5327–5338, 1982.

Chave, A.D., S.C. Constable, and R.N. Edwards, Electrical exploration methods for the seafloor, in *Electromagnetic Methods in Applied Geophysics,* vol. 2, edited by M. Nabighian, pp. 931–966, Soc. of Explor. Geophys., Tulsa, Okla., 1991.

Constable, S.C., Marine electromagnetic induction studies, *Surv. Geophys., 11*, 303–327, 1990.

Constable, S.C., Constraints on mantle electrical conductivity from field and laboratory measurements, *J. Geomagn. Geoelect., 45*, 707–728, 1993.

Constable, S.C., and G. Heinson, In defense of a resistive oceanic upper mantle: reply to a comment by Tarits, Chave and Schultz, *Geophys. J. Int., 114*, 717–723, 1993.

Constable, S.C., R.L. Parker and C.G. Constable, Occam's inversion: A practical algorithm for generating smooth models from EM sounding data, *Geophysics, 52*, 289–300, 1987.

Constable, S.C., T.J. Shankland and A. Duba, The electrical conductivity of an isotropic olivine mantle, *J. Geophys. Res., 97*, 3397–3404, 1992.

Cox, C.S., Electromagnetic induction in the oceans and inferences on the constitution of the earth, *Geophys. Surv., 4*, 137–156, 1980.

Cox, C.S., S.C. Constable, A.D. Chave, and S.C. Webb, Controlled source electromagnetic sounding of the oceanic lithosphere, *Nature, 320*, 52–54, 1986.

deGroot-Hedlin, C. and S.C. Constable, S.C., Occam's inversion and the North American Central Plains electrical anomaly, *J. Geomagn. Geoelect., 45*, 985–1000, 1993.

Evans, R.L., Constraints on the large-scale porosity and permeability structure of young oceanic crust from velocity and resistivity data, *Geophys. J. Int., 119*, 869–879, 1994.

Evans, R.L., S.C. Constable, M.C. Sinha, and C.S. Cox, Upper crustal resistivity structure of the East Pacific Rise near 13°N, *Geophys. Res. Lett., 18*, 1917–1920, 1991.

Evans, R.L., M.C. Sinha, S.C. Constable, and M.J. Unsworth, On the electrical nature of the axial melt zone at 13°N on the east Pacific rise, *J. Geophys. Res., 99*, 577–588, 1994.

Filloux, J.H., Magnetotelluric soundings over the northeast Pacific may reveal spatial dependence of depth and conductance of the asthenosphere, *Earth Planet. Sci. Lett., 46*, 244–252, 1980.

Filloux, J.H., Instrumentation and experimental methods for oceanic studies, in *Geomagnetism*, edited by J.A. Jacobs, pp. 143–248, Academic, San Diego, Calif., 1987.

Flosadottir, A.H. and S. Constable, Marine controlled source electromagnetic sounding 1. Modeling and experimental design, *J. Geophys. Res.*, this issue.

Glenn, W.E., and S.H. Ward, Statistical evaluation of electrical sounding methods, 1, Experimental design, *Geophysics, 41*, 1207-1221, 1976.

Grant, F.S. and G.F. West, *Interpretation Theory in Applied Geophysics*, McGraw-Hill, New York, 1965.

Heinson, G. and S.C. Constable, The electrical conductivity of the oceanic upper mantle, *Geophys. J. Int., 110*, 159–179, 1992.

Larsen, J.C., A new technique for layered earth magnetotelluric inversion, *Geophysics, 46*, 1247–1257, 1981.

Luther, D.S., J.H. Filloux and A.D. Chave, Low-frequency, motionally induced electromagnetic fields in the ocean 2. Electric field and Eulerian current comparison, *J. Geophys. Res., 96*, 12797–12814, 1991.

Oldenburg, D.W., K.P. Whittall, K.P. and R.L. Parker, Inversion of ocean bottom magnetotelluric data revisited, *J. Geophys. Res., 89*, 1829–1833, 1984.

Parker, R.L., The inverse problem of resistivity sounding, *Geophysics, 49*, 2143-2158, 1984.

Parker, R.L. and Whaler, K.A., Numerical methods for establishing solutions to the inverse problem of electromagnetic induction, *J. Geophys. Res., 86*, 9574–9584, 1981.

Pezard, P.A., Electrical properties of mid-ocean ridge basalt and implications for the structure of the upper oceanic crust in hole 504B, *J. Geophys. Res., 95*, 9237–9264, 1990.

Quist, A.S., and W.L. Marshall, Electrical conductances of aqueous sodium chloride solutions from 0° to 800° and at pressures to 4000 Bars, *J. phys. Chem., 71*, 684–703, 1968.

Sinha, M.C., P.D. Patel, M.J. Unsworth, T.R.E. Owen, and M.R.G. MacCormac, An active source electromagnetic system for marine use, *Mar. Geophys. Res., 12*, 59–68, 1990.

Smith, J.T., and J.R. Booker, Magnetotelluric inversion for minimum structure, *Geophysics, 53*, 1565–1576, 1988.

Smith, B.D., and S.H. Ward, On the computation of polarization ellipse parameters, *Geophysics, 39*, 867–869, 1974.

Steskey, R.M., and W.F. Brace, Electrical conductivity of serpentinized rocks to 6 kilobars, *J. Geophys. Res., 78*, 7614–7621, 1973.

Tarits, P., A.D. Chave and A. Schultz, Comment on 'The electrical conductivity of the oceanic upper mantle' by G. Heinson and S. Constable, *Geophys. J. Int., 114*, 711–716, 1993.

Unsworth, M., and D. Oldenburg, Subspace inversion of electromagnetic data: application to mid-ocean-ridge exploration, *Geophys. J. Int., 123*, 161–168, 1995.

Webb, S.C. and Constable, S.C., Microseism propagation between two sites on the deep sea floor, *Bull. Seismol. Soc. Am., 76*, 1433–1445, 1986.

Webb, S.C., S.C. Constable, C.S. Cox, and T. Deaton, A seafloor electric field instrument, *J. Geomagn. Geoelectr., 37*, 1115–1130, 1985.

Webb, S.C., X. Zhang, and W. Crawford, Infragravity waves in the deep ocean, *J. Geophys. Res., 96*, 2723–2736, 1991.

Young, P.D., and C.S. Cox, Electromagnetic active source sounding near the East Pacific Rise, *Geophys. Res. Lett., 8*, 1043–1046, 1981.

Zumberge, M.A., J.A. Hildebrand, J.M. Stevenson, R.L. Parker, A.D. Chave, M.E. Ander, and F.N. Speiss, Submarine measurement of the Newtonian gravitational constant, *Phys. Rev. Lett., 67*, 3051–3054, 1991.

C.S. Cox and S. Constable, University of California San Diego, Scripps Institution of Oceanography, Institute of Geophysics and Planetary Physics 0225, La Jolla, CA 92093-0225. (e-mail: sconstable@ucsd.edu, cscox@ucsd.edu)

(Received April 19, 1995, revised November 17, 1995, accepted November 21, 1995.)